

Human rhinovirus 3 at 3.0 Å resolution

Rui Zhao¹, Daniel C Pevear², Marcia J Kremer¹, Vincent L Giranda³, Jennifer A Kofron⁴, Richard J Kuhn¹ and Michael G Rossmann^{1*}

Background: The over 100 serotypes of human rhinoviruses (HRV) are major causative agents of the common cold in humans. These HRVs can be roughly divided into a major and minor group according to their cellular receptors. They can also be divided into two antiviral groups, A and B, based on their sensitivity to different capsid-binding antiviral compounds. The crystal structures of HRV14 and HRV16, major-receptor group rhinoviruses, as well as HRV1A, a minor-receptor group rhinovirus, were determined previously. Sequence comparisons had shown that HRV14 seemed to be an outlier among rhinoviruses. Furthermore, HRV14 was the only virus with no cellular ‘pocket factor’ in a hydrophobic pocket which is targeted by many capsid-binding antiviral compounds and is thought to regulate viral stability. HRV3, another major-receptor group virus, was chosen for study because it is one of a subset of serotypes that best represents the drug sensitivity of most rhinovirus serotypes. Both HRV3 and HRV14 belong to antiviral group A, while HRV16 and HRV1A belong to antiviral group B.

Results: Surprisingly, HRV3 was found to be very similar to HRV14 in sequence and structure. Like HRV14, crystallized HRV3 also has no bound pocket factor. The structure of HRV3 complexed with an antiviral compound, WIN56291, was also determined and found to be similar to the same antiviral compound complexed with HRV14.

Conclusions: The amino-acid sequence and structural similarity between HRV3 and HRV14 suggests that rhinoviruses in the same antiviral group have similar amino-acid sequences and structures. The similar amino-acid composition in the pocket region and the viral protein VP1 N termini in all known group B HRV sequences suggests that these viruses may all contain pocket factors and ordered N-terminal amphipathic helices in VP1. Both of these factors contribute to viral stability, which is consistent with the observations that group B rhinoviruses have a higher chance of successful transmission from one host to another and is a possible explanation for the observed higher pathogenicity of these rhinoviruses.

Introduction

Human rhinoviruses (HRV) are a genus of the picornavirus family and are the major causative agent of common colds. There are over 100 different serotypes, which can be divided into at least two groups [1]. The majority of HRVs (the major-receptor group viruses) use intercellular adhesion molecule-1 (ICAM-1) as a receptor [2,3] for cell attachment and entry. The remaining rhinoviruses (the minor-receptor group viruses), except for HRV87 [4], can utilize low density lipoprotein receptor molecules [5].

The single-stranded (+) RNA genome of HRVs is about 7.2kb in length and is encapsidated by a protein shell that has pseudo $T=3$ icosahedral symmetry. The diameter of the virus is about 300 Å, and the molecular weight is approximately 8.5×10^6 Da. The RNA genome directs the synthesis of a polyprotein, which is subsequently cleaved

into capsid proteins and nonstructural proteins. The viral capsid is made of 60 copies each of viral proteins VP1–VP4. VP1, VP2 and VP3 each have a molecular weight of about 30kDa; VP4 is a 7kDa small protein that lines the internal surface of the capsid. The crystal structures of HRV14 [6] and HRV16 [7], both belonging to the major-receptor group of rhinoviruses, and of HRV1A [8], belonging to the minor-receptor group of rhinoviruses, have been determined previously. Each of the viral proteins VP1, VP2 and VP3 is folded into an eight-stranded ($\beta\beta-\beta\text{I}$) antiparallel β -barrel motif which has a well conserved topology among picornaviruses. The eight β strands form two opposing sheets ‘BIDG’ and ‘CHEF’. The BIDG sheet faces mostly towards the viral interior, whereas the CHEF sheet is more exposed on the exterior of the viral surface. The barrel has a wedge shape, with the BC, HI, DE and FG loops forming the narrow end that points toward the icosahedral fivefold

Addresses: ¹Department of Biological Sciences, Purdue University, West Lafayette, IN 47907-1392, USA, ²ViroPharma Inc., 76 Great Valley Parkway, Malvern, PA 19355, USA, ³Department of Structural Biology, Abbott Laboratories, D-46Y AP10, 100 Abbott Park Road, Abbott Park, IL 60064-3500, USA and ⁴655 Main Street, Bolton, MA 01740, USA.

*Corresponding author.
E-mail: mgr@indiana.bio.purdue.edu

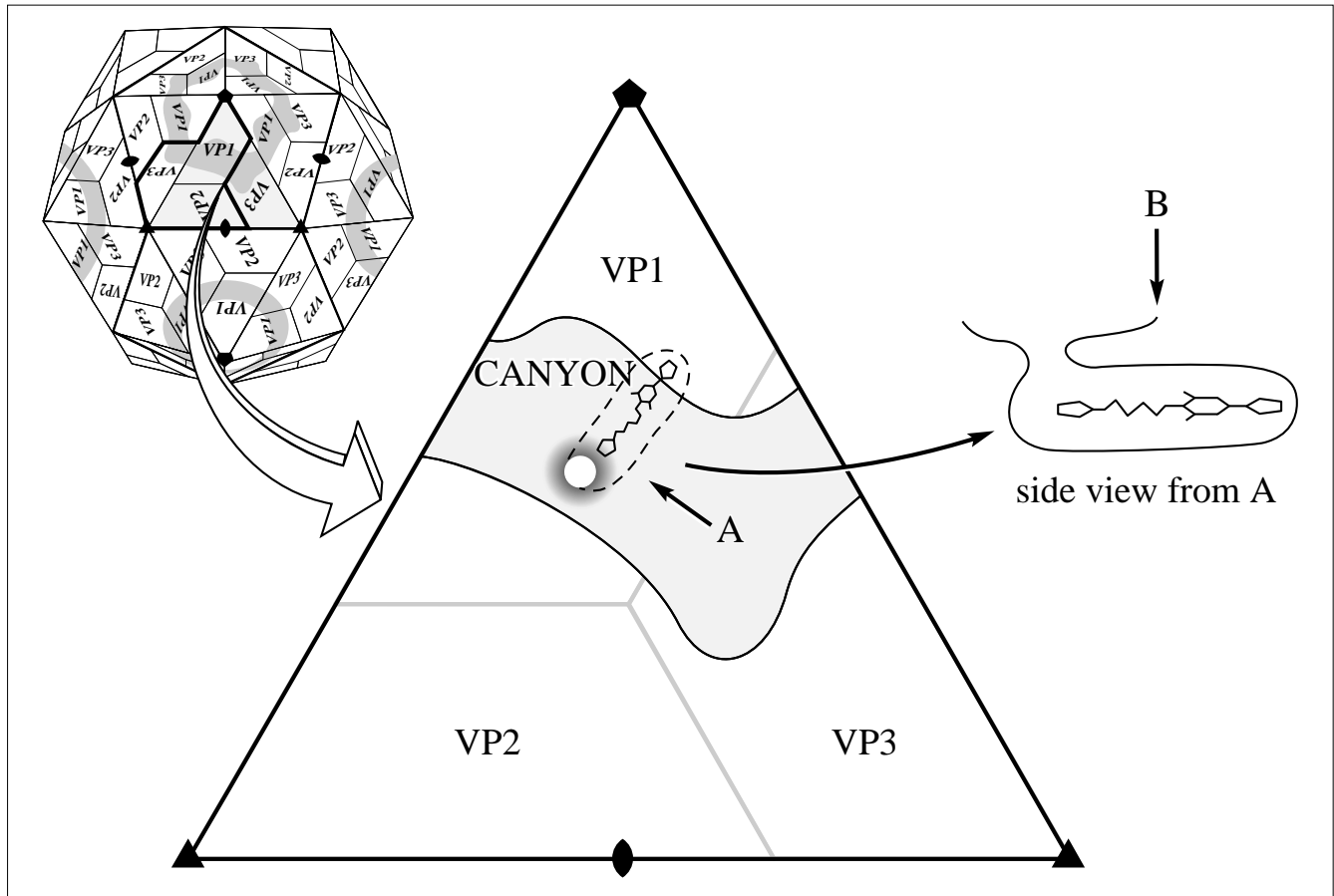
Key words: antigenicity, antiviral compounds, pocket factor, rhinoviruses, stability, structure

Received: 31 July 1996
Revisions requested: 28 August 1996
Revisions received: 9 September 1996
Accepted: 9 September 1996

Structure 15 October 1996, 4:1205–1220

© Current Biology Ltd ISSN 0969-2126

Figure 1



Diagrammatic view of picornavirus with enlargement of one icosahedral asymmetric unit showing the outline of the canyon and the entrance to the antiviral-binding pocket. The protomeric assembly unit (which differs from the geometric definition of the asymmetric unit) is

shown in heavy outline on the icosahedron. The arrow B shows the direction of view used in Figure 7. (The figure was adapted from Oliveira *et al.* [7], with permission.)

axes in the case of VP1 or towards the quasi-sixfold axes in the case of VP2 and VP3.

There is a 'canyon' with a depth of approximately 15 Å surrounding each of the icosahedral fivefold axes (Fig. 1). The floor of the canyon is mainly made of the GH loop in VP1. The 'north' rim of the canyon, closer to the viral fivefold axis, is formed exclusively by VP1. The GH loop in VP1, together with the C termini of VP1 and VP3, form the 'south' rim of the canyon, further away from the viral fivefold axis. Residues lining the canyon floor are more conserved than are other surface residues [9,10]. It was proposed that the cellular receptor would bind to residues on the canyon floor. These residues are inaccessible to antibodies due to steric hindrance and would, therefore, allow the virus to escape host immune surveillance [6,11]. This hypothesis was supported by site-directed mutagenesis of residues on the canyon floor [12] and was confirmed by cryoelectron microscopy of HRV16 complexed with

soluble ICAM-1 [13]. Furthermore, antibody molecules were demonstrated to bind on the canyon rim by analyzing antibody neutralizing escape mutations [14] and by cryoelectron microscopy of HRV14 complexed with neutralizing antibodies [15]. The escape mutations were clustered into four areas, the neutralizing immunogenic (NIm) sites IA, IB, II and III.

There is a hydrophobic pocket, between the BIDG and CHEF sheets of VP1, underneath the canyon (Fig. 1). A series of antiviral compounds designed by the former Sterling-Winthrop Pharmaceutical Company (WIN compounds) and other pharmaceutical companies bind into this pocket [16–18] and cause conformational changes of up to 4 Å for some Cα atoms in HRV14. However, in HRV16 and HRV1A, these compounds displace a previously resident 'pocket factor' (see below) and, hence, cause only small conformational changes. The WIN compounds can inhibit viral uncoating [16] and, in some cases,

also attachment to cells [19]. Rhinoviruses have been classified into antiviral groups A and B, based on their sensitivity to 15 antiviral compounds [20]. The minor-receptor group viruses all belong to antiviral group B (for example, HRV1A); however, the major-receptor group HRVs are scattered among antiviral groups A and B (for example, HRV14 and HRV3 belong to group A, whereas HRV16 belongs to group B). Viruses in group A are more sensitive to long antiviral compounds, whereas viruses in group B have greater sensitivity to short compounds.

In native HRV1A and HRV16, the pocket in VP1 is filled with electron density interpreted as either an eight-carbon [18] or twelve-carbon ([7]; AT Hadfield, personal communication) fatty acid (the ‘pocket factor’), based on its shape, the hydrophobic nature of the pocket and the polar environment at the pocket entrance. In HRV14, however, this pocket is empty. Similar pocket factors were observed in some other picornavirus structures, for example, a putative sphingosine or palmitate molecule in polioviruses (Mahoney type 1, Sabin type 3 and a chimeric type 2) [21–23], myristic acid in bovine enterovirus [24] and a putative palmitate molecule in coxsackievirus B3 [25]. No data are available as to the exact chemical identity of the pocket factor, although there is evidence for binding of myristic acid to bovine

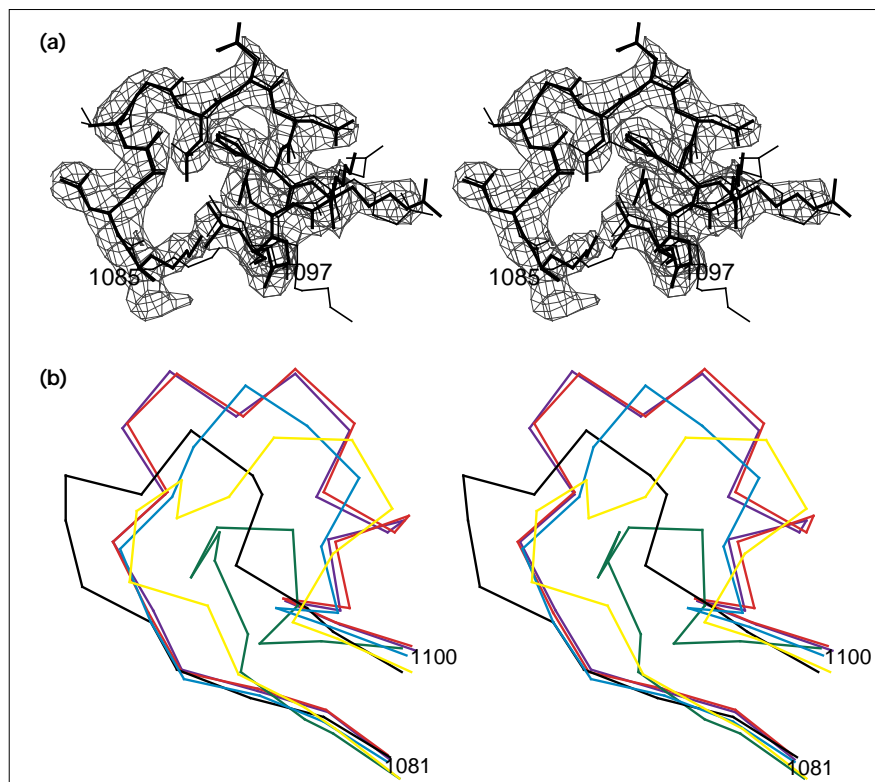
enterovirus. When WIN compounds or shorter WIN compound fragments, mimicking the pocket factor, bind into this pocket, they stabilize the virus to acidification [26] and heating [27–29]. It has been proposed that the pocket factor stabilizes the virion for transport between hosts, while it is displaced by the receptor during cell entry in preparation for uncoating [7,11]. This is equivalent to stabilizing proteins by filling hydrophobic holes with hydrophobic residues or compounds [30–32].

When rhinoviruses bind to cells, they are first converted to ‘A’ (‘altered’) particles which lack VP4 [33–35]. Subsequently, the A particles lose RNA and form empty particles. The A particles are hydrophobic [35,36], and their formation in polioviruses is associated with the externalization of the N terminus of VP1 [37].

The initial motivation for studying HRV3 was that this virus was used by the Sterling-Winthrop Pharmaceutical Company as one of a subset of serotypes that best represents the drug sensitivity of most rhinovirus serotypes [38]. We report here the nucleotide sequence determination of the HRV3 genome corresponding to the capsid proteins, the structure determination of HRV3 at 3.0 Å resolution and the structure determination of the complex of HRV3 with antiviral compound WIN56291. The same

Figure 2

The BC loop in VP1. **(a)** HRV3 electron density for the BC loop of VP1 (residues 1085–1098). The structure in HRV3 is shown with a thick line and that for HRV14 is shown with a thin line. **(b)** Different lengths and conformations of the BC loop of VP1 in HRV3 (purple), HRV14 (red), HRV16 (green), HRV1A (yellow), polio1 (black) and polio3 (blue).



compound had previously been studied when complexed to HRV14, HRV16 and HRV1A [7,18].

Results and discussion

Quality of the HRV3 electron-density map

The good quality of the HRV3 electron-density map at 3.0 Å resolution was indicated by the differentiation of residues that differed between HRV3 and HRV14 (Fig. 2a). Because of the presence of the noncrystallographic symmetry, a true measure of error in the electron density can be computed as the root mean square (rms) standard error, σ , between noncrystallographic symmetry related electron density. The value of σ found in this way was about one-third of the electron density rms deviation from zero. The maximum density for most of the main-chain atoms was around 10σ above zero, the mean level of the map. However, residues 1216–1223 (amino acid sequence numbers start with 1000, 2000, 3000 and 4000 for VP1, VP2, VP3 and VP4, respectively), in the GH loop of VP1, had density weaker than 6σ above the mean level of the map and their side-chain density was also weak and diffuse, indicating the flexibility of the GH loop in HRV3. The N-terminal residues 1001–1015, 2001–2007 and 4001–4025 could not be seen at any level. Uninterpretable, noise

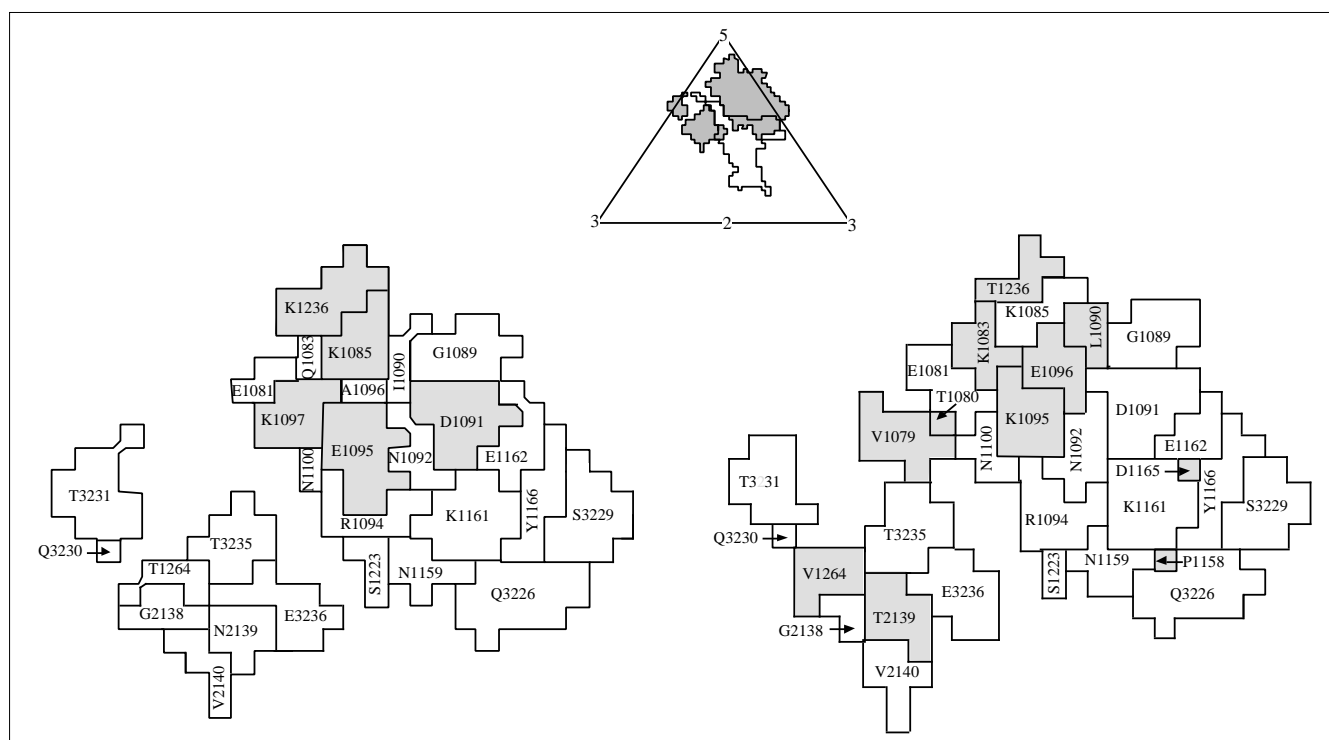
features started to appear at about 2σ above the mean level of the map.

The antigenic surface

Although the amino-acid sequences of HRV14 and HRV3 have considerable similarity (88% amino-acid sequence identity in the structural proteins), they are serologically distinguishable. Consequently, there should be some difference in the amino acids on the viral surface, especially those which represent the four primary antigenic epitopes, namely NIm IA, IB, II and III in HRV14. Out of the 106 residues that differ between HRV3 and HRV14, 60 are located on the viral surface. Furthermore, the antigenic BC loop of VP1, which forms much of the NIm IA epitope, is particularly variable in length and sequence among rhinoviruses and polioviruses (Fig. 2b). It has been used extensively for making chimeric viruses and altering the serological types of polioviruses [23,39–44]. Although there is little difference in conformation of this loop between HRV3 and HRV14 (Fig. 2a), the amino-acid sequence is rather different:

HRV3: K N A A G L D N H R K E G L
HRV14: K D A T G I D N H R E A K L

Figure 3



Diagrammatic view of the canyon (arbitrarily demarcated by a 146 Å radial distance from the viral center) and the Fab17 footprint (shaded area; top panel). Also shown are enlarged views of residues in the Fab17 footprint on HRV14 (left panel) and their corresponding

residues in HRV3 (right panel). Charged residues, proposed to be important in the antibody–virus interaction, are shown as shaded areas in the left panel. Residues in HRV3 which differ from those in HRV14 are shown as shaded areas in the right panel.

The NIm site IA and its area of interaction with a neutralizing antibody has been mapped in a study of the complex of the antibody fragment Fab17 with HRV14 [15]. The complementarity of charge between Fab17 and viral surfaces was proposed to be a major contribution to the binding energy [15]. Some of the residues involved in HRV14–antibody charge interaction have changed in HRV3 (Fig. 3), thus altering the requirements for neutralizing antibodies binding to epitope IA.

The other three NIm sites, IB, II and III, have not been studied as carefully as IA. The only available information relates to escape mutations in HRV14 to neutralizing antibodies. Although the mutated residues identify a central portion of the antigenic epitope, the extent of the surface covered by the bound antibody remains unknown. Nevertheless, comparison of the escape mutations in HRV14 with the sequence of HRV3 shows that HRV3 has changes in each of the four NIm sites and that, in many cases, HRV3 has the sequence of an escape mutation (Table 1). This demonstrates that the set of neutralizing antibodies for HRV3 is non-overlapping with that for HRV14.

VP4 and the N-terminal end of VP1

The differences between rhinoviruses are mainly located on the external surface loops or the internal capsid surfaces, in particular the conformation of VP4 and the N terminus of VP1 (Table 2). The structure of VP4 and the N terminus of VP1 can be roughly divided into three types represented by HRV3 or HRV14, by HRV1A or HRV16,

and by polio1 or polio3 (Fig. 4a). Of particular interest is the disordered N-terminal end of VP1 in HRV3 or HRV14 compared with the amphipathic helix that occurs in HRV1A or HRV16, or the strand of a β sheet that occurs in polio1 or polio3. The hydrophobic side of the helix in HRV16 mainly interacts with the ten-stranded β barrel formed by the N termini of VP4. The hydrophilic side of this helix faces the viral interior. The preference for the N termini of VP1 to form an amphipathic helix in HRV16 and HRV1A is apparent in helical wheel plots (Fig. 4b). The amphipathic character of this region is disrupted to a certain extent in HRV14, HRV3 (Fig. 4b), polio1 and polio3 [37]. The hydrophobic characteristics of the VP1 N-terminal residues are well conserved among all antiviral group B rhinoviruses such as HRV16 and HRV1A (Fig. 4c), suggesting that these viruses may all form N-terminal amphipathic helices in VP1.

The N terminus of VP4 forms two β strands of a ten-stranded β barrel surrounding the fivefold axis in HRV16 or forms two β strands of a three-stranded β sheet in polio1 and polio3 (Fig. 4a). The N terminus of VP4 is disordered in HRV1A, HRV14 and HRV3. However, there is density in HRV3 at a 2σ level, which might correspond to the extreme N terminus of VP4 (possibly residues 4003–4006) and form a β sheet with residues 4026–4029. Similar density features are also visible at low contour levels in the electron density of HRV1A and HRV14, although they are less obvious than that in HRV3. The N terminus of VP4 is myristylated in many picornaviruses and may play a role in viral assembly by stabilizing the pentamers and in viral penetration of membranes [45,46]. The myristate is visible in the electron density of HRV16 (AT Hadfield, RZ and MGR, unpublished results), poliovirus [22] and coxsackievirus B3 [25]. There is density which might correspond to the myristate attached to VP4 in HRV1A [8].

The ambivalence between disordered (HRV14 and HRV3) and ordered (HRV16 and to some extent HRV1A) helical structures in the N-terminal residues of VP1 may represent different points of equilibrium in the capsid assembly, giving the virion different degrees of stability prior to cell entry and disassembly. The binding of the N-terminal helix in VP1 to VP4 in HRV16 may increase the stability of the virus as it would stabilize the myristate cluster and hinder the ejection of VP4 on binding to cells or soluble ICAM-1. This is consistent with the greater stability of HRV16 compared with HRV3 and HRV14 [35]. In this case, the hydrophobic contacts between the VP1 helix and VP4 restrain the release of VP4 from the virion. Even more dramatically, when the C-terminal end of VP4 is covalently attached to the N-terminal end of VP2 in a maturation cleavage deficient mutant, the release of VP4 is inhibited, resulting in non-infectious particles [47].

Table 1

Escape mutations in the HRV14 NIm sites and their corresponding residues in HRV3.

NIm sites	Residues in HRV14	Escape mutations	Corresponding residues in HRV3
IA 1091	D	A E G H N V Y	D
	1095	G K	K [†]
IB 1083	Q	H	K
	1085	N	K
	1138	E G	E [†]
	1139	P	A
II 2158	S	F	T
	2159	V	V [†]
	2161	D V* D* K	V [†]
	2162	M A*	A [†]
	1210	D*	D [†]
	2136	G	E
III 3072	N	I	H
	3075	G K M	R
	3078	K V	E
	1287	I	K
	3203	D	G

*Mutants with double mutations: V2161 and A2162; D2161 and D1210. [†]Residues in HRV3 that are identical to the escape mutations in HRV14.

Table 2

Comparison of VP4 and N termini of VP1 in several different picornaviruses.

	HRV14	HRV3	HRV16	HRV1A	Polio1	Polio3
Number of amino acids in VP1	289	288	285	287	302	302
Regions of VP1 visible in the electron-density map	1014–1289	1016–1288	1001–1285	1005–1287	1006–1010 1020–1302	1007–1010 1024–1302
Conformation of the N terminus of VP1	disordered	disordered	1001–1012 forms an α helix which interacts with the N terminus of VP4	1005–1012 forms an α helix	1006–1010 and 4002–4006 form two parallel β strands	1007–1010 and 4003–4006 form two parallel β strands
Number of amino acids in VP4	68	68	68	68	68	68
Regions of VP4 visible in the electron-density map	4029–4068	4026–4068	4001–4007 4023–4044	4026–4044	4002–4016* 4023–4069	4002–4016* 4023–4069
Conformation of the N terminus of VP4	disordered	disordered	4001–4007 and 4023–4038 form two antiparallel β strands	disordered	4003–4006 and 4027–4030 form two antiparallel β strands	4003–4006 and 4027–4030 form two antiparallel β strands
Myristate on VP4	disordered	disordered	ordered	disordered	ordered	ordered

*4001 is the myristate attached to VP4.

Ca²⁺ binding

The DE loop of VP1 is involved in the interaction with a putative Ca²⁺ ion on the viral fivefold axis in all analyzed rhinoviruses [48]. A density peak, about three-fifths of the height of the protein density, is located at the putative Ca²⁺ ion position in HRV3. The ion is approximately 155 Å away from the viral center and forms a pentagonal bipyramid structure with seven ligands. It interacts with the five symmetry-related main-chain carbonyl oxygens of Ser1141 at an ion–ligand distance of 3.0 Å. Two water molecules are situated on the fivefold axis ‘above’ and ‘below’ the ion at a distance of 2.3 and 3.7 Å, respectively (‘above’ and ‘below’ indicate the direction toward the exterior and interior of the virus, respectively). With the exception of the water molecule at 2.3 Å, these liganding distances are far longer than those observed for many other Ca²⁺-binding sites, showing that the affinity of Ca²⁺ at this site is low. Nevertheless, the presence of Ca²⁺ at this site is demonstrated in that similar ions in HRV14 and HRV16 are EGTA chelatable [48]. These ions in rhinoviruses, as in many metalloproteins, may play a role in regulation of stability. However, the loss of the ion itself seems not to be enough to lead to viral disassembly as no conformational changes were observed in the EGTA-treated virus structures.

RNA structure

There is a weak (about 2 σ ; see section on ‘Quality of the HRV3 electron-density map’ for definition of σ) plate-like density near residue Trp2038 within the viral cavity. This

density is similar to that assigned as an RNA base in HRV14 [49], HRV16 (AT Hadfield, RZ and MGR, unpublished results), poliovirus [22] and coxsackievirus B3 [25]. It forms a stacking interaction with Trp2038. Residue 2038 is conserved in all rhinoviruses of known sequence and may, therefore, be important in interacting with RNA and may help RNA packaging. Site-directed mutagenesis of this residue to alanine, valine or histidine in HRV16 is lethal (W-M Lee, personal communication).

The site for receptor attachment in the canyon

Fourteen of the 18 residues in the footprint of ICAM-1 on HRV14 are the same in HRV3. The four different residues are away from the center of the ICAM-1 footprint (Fig. 5) and expose one additional residue in HRV3. As a first approximation, IC₅₀ (the concentration of soluble ICAM-1 that inhibits 50% of the rhinovirus infectivity) of ICAM-1 for different rhinoviruses is reciprocally proportional to the affinity constant of ICAM-1 to these viruses. The difference in IC₅₀ between HRV3 (4.6 ± 1.5 μ M) and HRV14 (3.3 ± 0.5 μ M) [50] is not significant, indicating that the above residues are not critical for ICAM-1 binding.

Conformation of WIN56291 when complexed with HRVs

The HRV3–WIN56291 complex (Fig. 6) shows continuous electron density for most of the main-chain atoms. The side chains are also mostly well defined. However, residues 1218, 1219 and 1220, in the GH loop that forms part of the antiviral-binding pocket, have somewhat diffuse density

Figure 4

Structure of the N terminus of VP1. (a) Stereodiagram showing different conformations of VP4 and the N termini of VP1 in HRV14 (red), HRV16 (green) and polio1 (black). Shown also are the radial distances from the viral center along the fivefold axis. The external surface of the virion is at a radius of about 150 Å. (b) The N-terminal residues of VP1 displayed on helical wheels. Red, blue and black represent hydrophilic, hydrophobic and glycine residues, respectively. Residues in HRV1A or HRV3 which differ from those in HRV16 or HRV14 are shown in parenthesis. Residues surrounding the HRV16 helical wheel are the VP4 residues which interact with the VP1 helix in HRV16. (c) Amino acid sequence alignment of the N termini of VP1 in rhinoviruses.

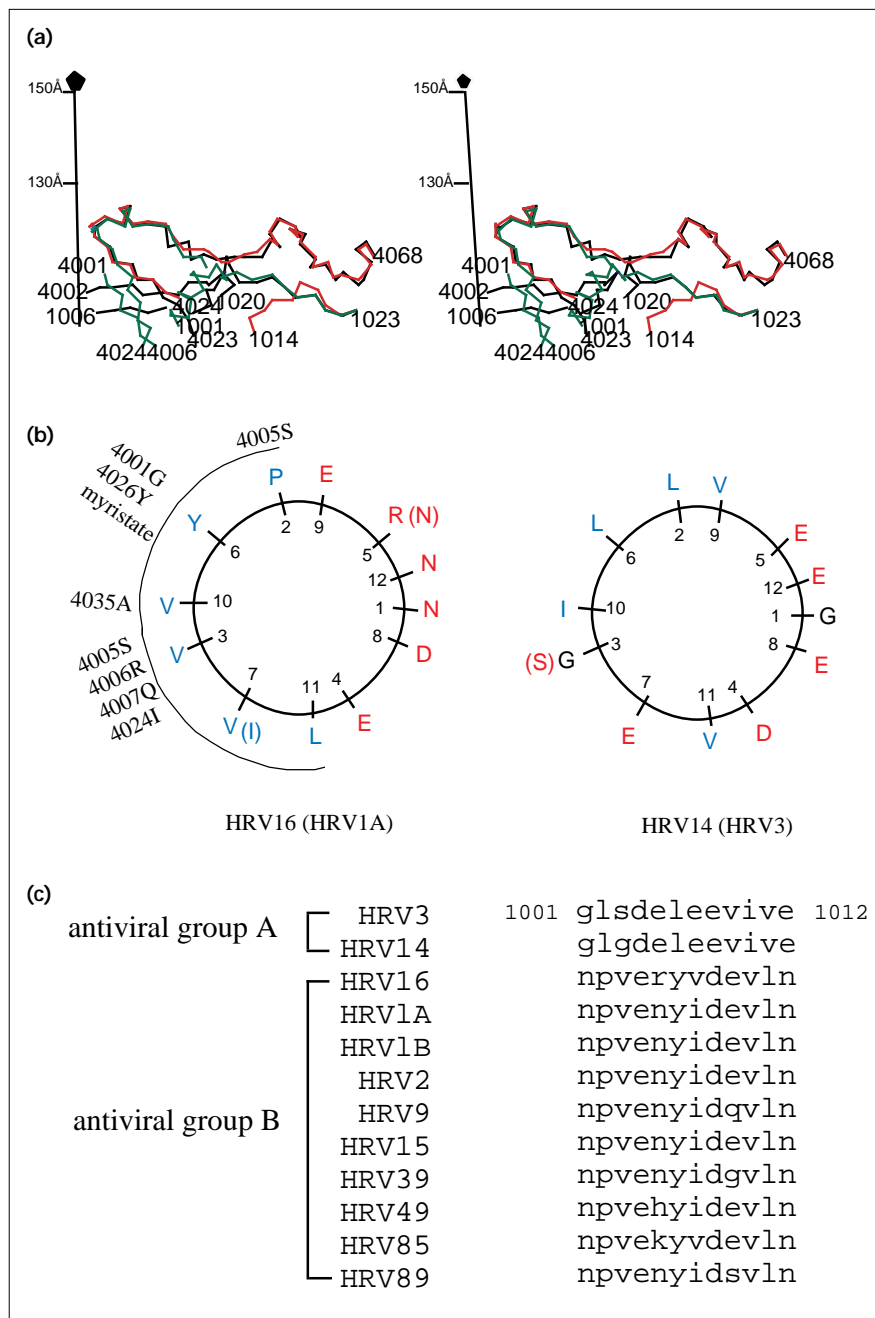
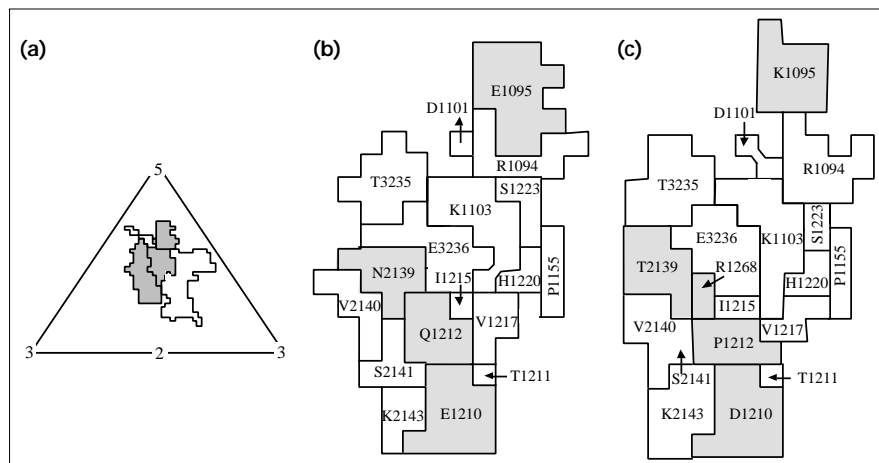


(Fig. 6b). These residues also have diffuse densities in the uncomplexed structures, suggesting that the GH loop is rather flexible.

The density corresponding to the WIN56291 compound is well defined (Fig. 6b). The oxazoline and phenoxy rings lie in slightly flattened density and are coplanar. The two chlorines on the phenoxy ring are seen as two large bulges. The isoxazole ring at the other end of the molecule is almost

perpendicular to the plane of the phenoxy and oxazoline rings. The conformation of WIN56291 and its position within the HRV3 drug-binding pocket is essentially the same as it is in HRV14 (Fig. 7a). The conformations and binding sites of this compound in HRV16 and HRV1A have greater similarity to each other than to those in HRV14 and HRV3 (Fig. 7a). The principal difference in the drug conformation between HRV3 and HRV16 is the bend of the aliphatic chain (Fig. 7a,b). Tyr1128 and Met1224 in HRV3

Figure 5



Footprint of the receptor on the viral surface. (a) Diagrammatic view of the canyon and the ICAM-1 footprint (shaded area). (b,c) Enlarged views of residues in the ICAM-1 footprint on HRV14 (b) and their corresponding residues in HRV3 (c). Residues that differ between HRV3 and HRV14 are shown as shaded areas in (b) and (c).

(corresponding to Ile1122 and Leu1217 in HRV16) cause a bend at the second carbon atom (C2#) in the aliphatic chain and the compound to be translated approximately 2 Å further into the pocket and about 1 Å perpendicular to its length. The translation further into the pocket in HRV3, together with the smaller residue Cys1199 (compared with a methionine in HRV16) at the other end of the pocket, creates too much space for shorter compounds such as WIN56291. This is consistent with the larger MIC₅₀ (MIC₅₀ is the minimum concentration of WIN compound which inhibits 50% of the rhinovirus infectivity in cell culture) values for WIN56291 in HRV3 compared with HRV16 (Fig. 6c). Some drug-resistant mutants of HRV14, selected in the presence of long WIN compounds (with seven-carbon aliphatic chains), have Cys1199 replaced by tyrosine or tryptophan [28], thus inhibiting drug entry into the pocket. However, these mutants have less resistance to shorter compounds, demonstrating the role of Cys1199 in controlling compound length.

All of the group B rhinoviruses with known sequence have similar amino acids forming the drug-binding pocket (Table 3). Group B rhinoviruses contain small isoleucine, valine or leucine residues in place of Tyr1128 or Met1224 in HRV3, but contain a bulky methionine residue in the position of Cys1199. These three residues appear to be the major determinants that control different preferred lengths and conformations of antiviral compounds.

Polioviruses were also associated with group A by Andries *et al.* [20]. However, residues comprising the pocket of poliovirus not only differ from group B rhinoviruses, but also differ considerably from group A rhinoviruses (Table 3). In spite of this, long compounds, such as WIN51711, are preferred by polioviruses and bind in similar conformations to those binding to group A rhinoviruses (Fig. 7c) [51]. Thus, common features must

exist in the pockets of rhinoviruses and polioviruses that contribute to the similar drug lengths and conformations preferred by these viruses. One important feature is the existence of a large residue in all group A rhinoviruses and polioviruses (tyrosine, phenylalanine or leucine) at the position of 1128 in HRV14, whereas in group B the corresponding residue is smaller (isoleucine or valine). In group A viruses, this residue causes a kink in the aliphatic chain of bound antiviral compounds, whereas in group B viruses the drug binds in a relatively linear fashion. The length of the drug may be controlled by a number of factors common to polioviruses, HRV14 and HRV3. The large residue (Tyr1128 in HRV14 and HRV3) will tend to force the large aromatic portion of the drug further into the available space of the pocket to avoid steric hindrance. The pore end of the pocket, determined in part by residue 1199 (HRV14 and HRV3 numbers), is somewhat different between polioviruses and the group A rhinoviruses, but both sets of structures allow for fairly long antiviral compounds.

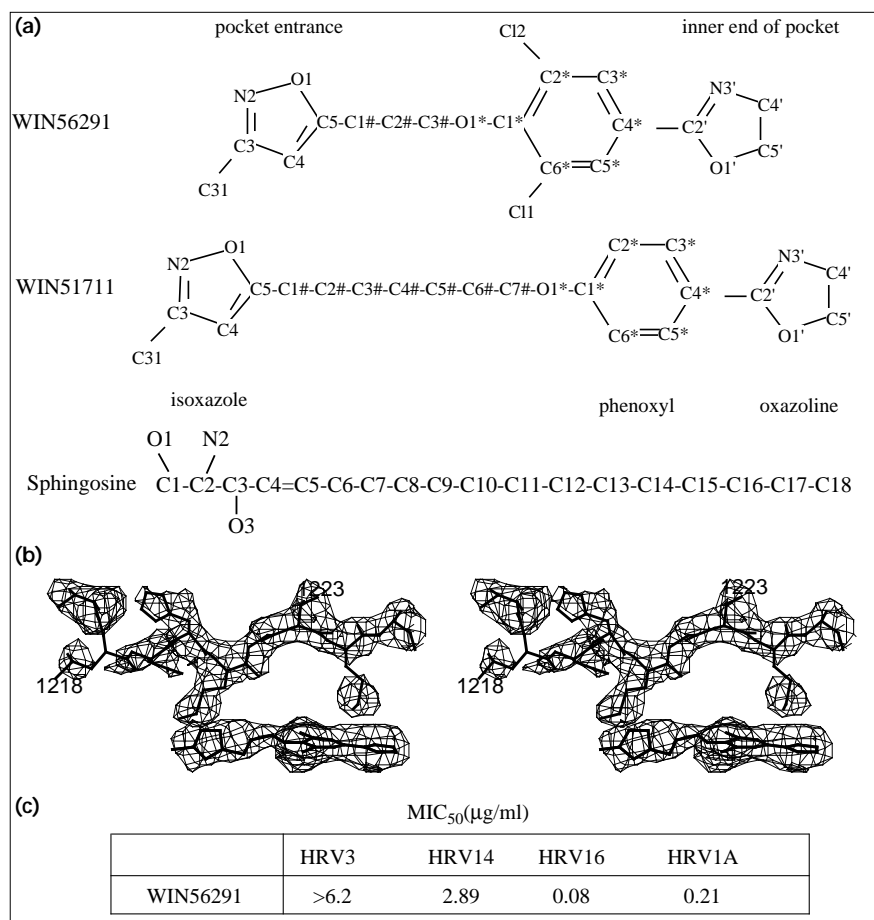
Conformational changes of the virus induced by WIN56291

Antiviral compounds displace the naturally occurring pocket factor in HRV16, HRV1A, coxsackievirus B3 and polioviruses. This is particularly well demonstrated by the electron-density map of coxsackievirus B3 complexed with a compound shorter than the pocket factor, as there is no trace of the pocket factor in those regions not occupied by the compound. In the above-mentioned viruses, the conformational changes produced by the displacement of pocket factor are quite small, being mostly less than 1.2 Å [18].

In contrast, the conformational changes are much larger when antiviral compounds bind to HRV3 or HRV14, which have no pocket factor in the purified virus used for crystallization and in which the pocket is collapsed. In these

Figure 6

Capsid-binding antiviral compounds. (a) Structures of WIN56291, WIN51711 and a sphingosine molecule. (b) Electron density for the HRV3–WIN56291 complex showing the flexible GH loop and the WIN compound conformation. (c) MIC₅₀ values for WIN56291.



viruses, the antiviral compounds must enlarge the pocket's volume to permit entry. When WIN56291 binds to HRV3, the largest changes occur in the GH loop, including residues 1212–1225, where the C α atom of 1217 moves 4.4 Å. Other large conformational changes, with displacements of C α atoms as large as 0.9 Å, occur between residues 1152–1157 in the EF loop and between residues 1103–1107 in the loop between the β C strand and the α A helix. Some very minor changes that have less than 0.6 Å displacement of C α atoms, although with uncertain significance, occur between residues 1126–1129 in β D, 1186–1191 in β G, and 1197–1200 also in β G. The conformational changes that occur when WIN56291 binds to HRV3 and HRV14 are similar, consistent with the similar MIC₅₀ values for this compound in these two viruses (Fig. 6a).

The pocket and pocket factor

The crystal structures of HRV3 and HRV14, unlike other rhinoviruses, polioviruses, bovine enterovirus and coxsackievirus B3, do not contain pocket factors in their hydrophobic pockets. It has been proposed that there is a loosely bound cellular pocket factor in HRV14, which is extracted

during the purification procedure [7,11]. Presumably, the absence of the pocket factor in HRV3 and HRV14 is due to differences in residues lining the pocket compared with other rhinoviruses and polioviruses.

There are three kinds of pockets in rhinoviruses and polioviruses, as represented by group B rhinoviruses, group A rhinoviruses and group A polioviruses. Group B rhinoviruses prefer short antiviral compounds and short pocket factors. Both group A rhinoviruses and polioviruses prefer long antiviral compounds, but group A polioviruses contain long pocket factors, whereas group A rhinoviruses do not contain any pocket factor. The position and conformation of WIN compounds within the pocket mimics the position and conformation of the respective pocket factor in polioviruses and group B rhinoviruses (Fig. 7d). As WIN compounds bind similarly in polioviruses and HRV14, and as polioviruses contain a long pocket factor, it seems reasonable that a long pocket factor would also be able to bind in HRV14 or HRV3. However, a pocket factor is different from a WIN compound in that it has a much smaller volume, as it does not have the ring structures at both ends

Figure 7

Comparison of the binding mode of antiviral compounds in different rhinoviruses. The orientations of all parts of this figure are identical and are illustrated in Figure 1.

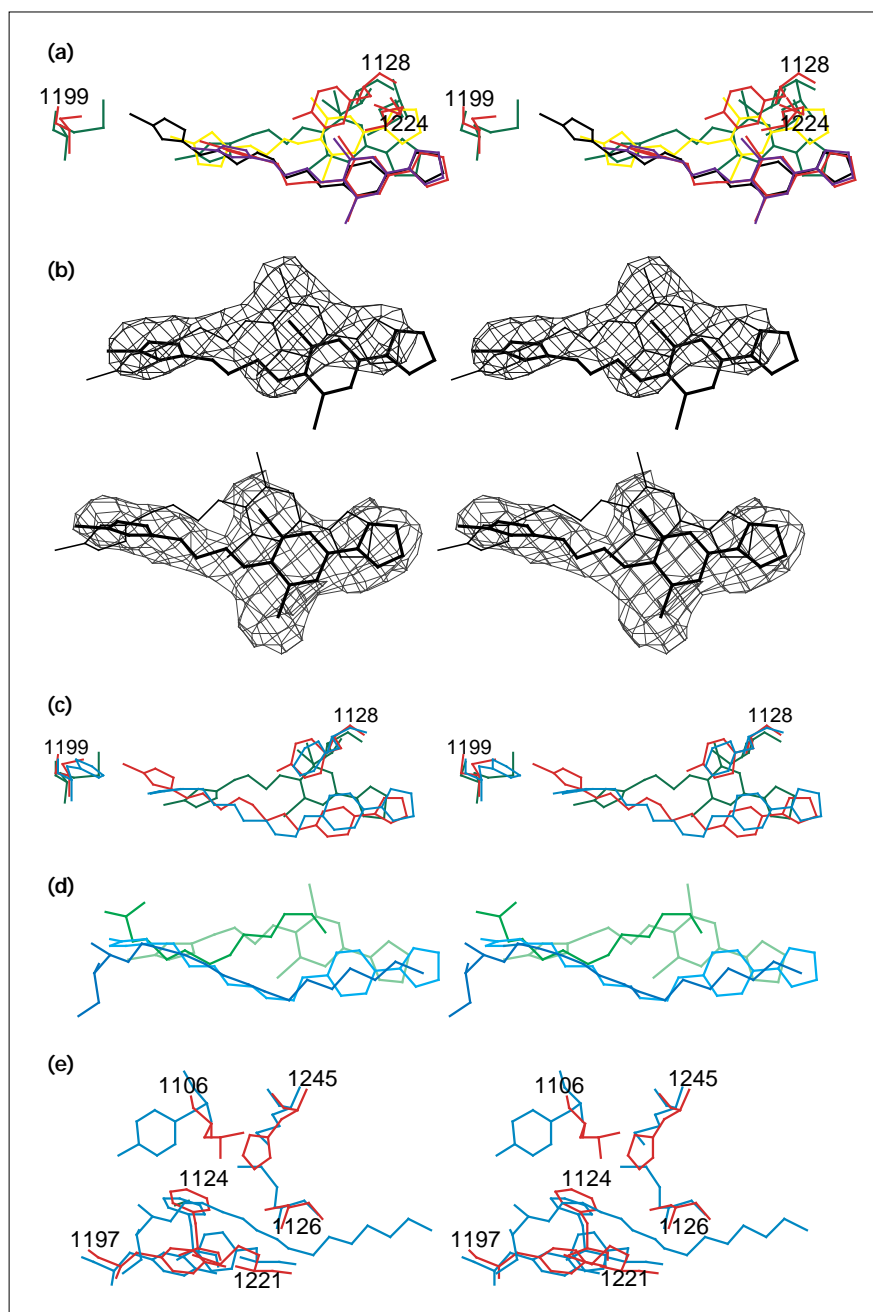
(a) Different conformations of WIN56291 in HRV3 (purple), HRV14 (red), HRV16 (green) and HRV1A (yellow), and residues causing these different conformations. The conformation of a long compound, WIN51711, in HRV14 is shown in black.

(b) Electron densities of WIN56291 in HRV16 (top) and HRV3 (bottom) superimposed with the WIN56291 structures in HRV16 (thin line) and HRV3 (thick line), demonstrating the bent conformation and translation of WIN56291 in HRV3 compared with HRV16.

(c) Residues contributing to the similar conformation of WIN51711 in polio3 (blue) compared with HRV14 (red). The corresponding residues and the different conformation of WIN56291 in HRV16 are also shown (green).

(d) Positions and conformations of WIN56291 (green) and the pocket factor (dark green) in HRV16, as well as WIN51711 (light blue) and the pocket factor (dark blue) in polio3, showing the similar position and conformation between pocket factors and WIN compounds.

(e) Residues important for binding pocket factor in polio3 (blue) compared with the structure of HRV14 (red) when complexed with WIN51711.



of the molecule. Thus, it may be especially important to have a narrow and hydrophobic pocket to maximize the interaction between the virus and the pocket factor. Polioviruses seem to form a better binding environment for pocket factor than HRV14 or HRV3, according to this criteria (Fig. 7e). In HRV14 or HRV3, residues His1245 and Ser1126 (Table 3) make the middle part of the pocket broader and more polar than polioviruses, which is not the most suitable binding environment for an aliphatic chain [51]. Furthermore, in the region close to the pore, residues

Leu1106 and Met1221 in HRV14 or HRV3 are replaced by either a tyrosine or a phenylalanine in all polioviruses. These two aromatic residues in polioviruses (Table 3), together with residues Phe1130 and Tyr1205, interact extensively with atoms C3–C7 (Fig. 6a) of the sphingosine pocket factor, which may also contribute to the favorable binding of a pocket factor.

Sequence information [20,52,53] shows that rhinoviruses belonging to the same antiviral group share significant

Table 3

Equivalent residues that line the antiviral-binding pocket in different picornaviruses.*

Group A HRV		Group B HRV [†]		Group A polio [†]	
HRV14 or HRV3	HRV16	Nine other rhinoviruses [‡]		Polio1	Polio3
I1104	I1098	8I, 1V		I1110	I1110
L1106	L1100	7L, 2I		Y1112	Y1112
F1124 [§]	F1118	9F		F1130	F1130
S1126 [§]	S1120	9S		M1132	M1132
Y1128	I1122	9I		L1134	F1134
A1150	Y1142	8Y, 1F		I1157	I1157
Y1152	Y1144	9Y		Y1159	Y1159
P1174	A1166	7A, 2M		P1181	P1181
V1176	V1168	5V, 4I		I1183	I1183
F1186	F1179	9F		I1194	I1194
V1188	L1181	8L, 1I		V1196	V1196
V1191	L1184	8L, 1M		V1199	V1199
Y1197	Y1190	9Y		Y1205	Y1205
C1199	M1192	9M		H1207	H1207
N1219	N1212	9N		N1235	D1236
M1221	M1214	9M		F1237	F1238
M1224	L1217	6L, 3I		L1240	L1241
H1245 [§]	H1238	9H		L1261	M1262
A3024	A3024	9A		A3024	A3024

*The structure of HRV14 complexed with WIN51711 was used to select these residues. [†]Bold type indicates residues that are different from those of HRV14. [‡]The nine group B rhinoviruses are HRV1A, HRV1B, HRV2, HRV9, HRV15, HRV39, HRV49, HRV85 and HRV89. Residues without [§] have at least one atom located within 4.0 Å from

WIN51711. Note that residues A1150 and P1174 have only main-chain atoms closer than 4.0 Å to WIN51711. Residues with [§] were selected because their equivalent residues in polio3 are in the vicinity of either WIN51711 or the sphingosine pocket factor, although they are at a distance greater than 4 Å from WIN51711 in HRV14.

amino-acid sequence similarities, especially in the pocket region (Table 3). Thus, group B rhinoviruses may all favor the binding of a short pocket factor, while group A rhinoviruses are likely to bind loosely to a pocket factor as in HRV14 and HRV3. On the other hand, polioviruses, having a pocket different from either group A or group B rhinoviruses, favor the binding of a long pocket factor.

The stability difference between HRV16 and HRV14 or HRV3
HRV16 is more stable than both HRV3 and HRV14 when treated with soluble ICAM-1 or at low pH [35]. The better binding of a pocket factor and the interaction of VP4 with the amphipathic helix at the N terminus of VP1 are stabilizing factors in HRV16.

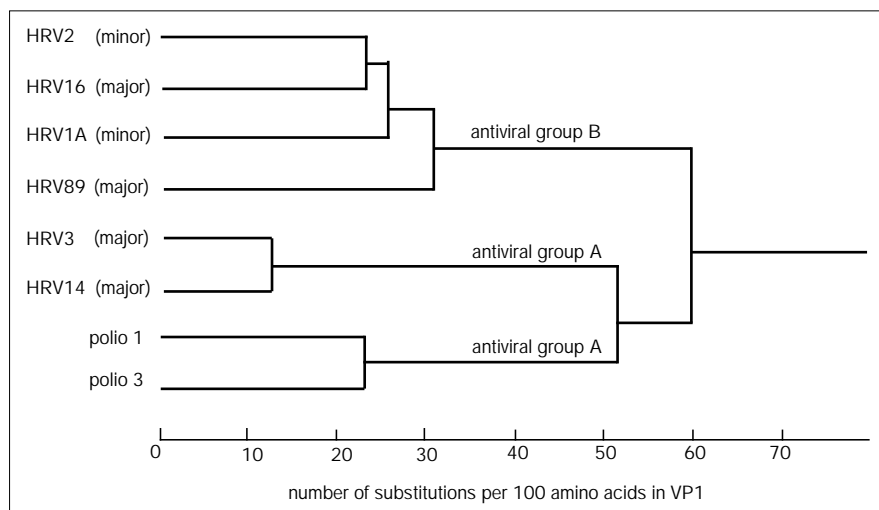
Andries *et al.* [20] noticed that viruses in antiviral group B accounted for five times as many clinical colds as viruses in group A. Taking into account that there are twice as many viruses in group B as in group A, viruses in group B still account for at least twice as many clinical infections as those in group A. It was suggested that 'something in the structure of antiviral group B viruses endows them with a higher pathogenicity' [20]. As discussed earlier, viruses in group B may all contain pocket factors and amphipathic helices in the N termini of VP1, and both of these factors contribute to the viral stability. This may permit group B viruses to have a higher chance of successful transmission from one host cell to another and lead to a higher pathogenicity.

Table 4

Percentage of amino acid sequence identity between different picornaviruses in the whole structural protein region (above the diagonal) and in the VP1 region (below the diagonal).

Virus	Antiviral group A		Antiviral group B		Antiviral group A	
	HRV3	HRV14	HRV16	HRV1A	Polio 1	Polio 3
HRV3		88	52	51	50	49
HRV14	85		52	51	50	50
HRV16	42	43		80	49	50
HRV1A	41	42	71		48	48
Polio 1	46	46	41	39		82
Polio 3	45	46	41	38	76	

Figure 8



A phylogenetic tree for rhinoviruses and polioviruses based on amino acid sequence similarities in VP1. Distances between different viruses were calculated using the UWGCG (University of Wisconsin Genetics Computer Group) DISTANCES program. Besides viruses with known structure, two more rhinovirus serotypes (HRV2 and HRV89) were used in the phylogenetic tree to demonstrate that the use of specific receptors by rhinoviruses may have had a number of independent origins.

The evolution of rhinoviruses and polioviruses

HRV14 has long been considered an outlier among rhinoviruses based on sequence comparisons [52]. It was, therefore, surprising to find that the amino-acid sequences of the structural proteins in HRV3 and HRV14 were 88% identical. It is noteworthy that HRV14 and HRV3 both belong to antiviral group A. Furthermore, the partial amino-acid sequence (VP2 region) of another group A rhinovirus, HRV72, has an identity greater than 84% with both HRV14 and HRV3 [53]. On the other hand, the VP2 sequences of 18 group B rhinoviruses, including HRV16 and HRV1A, showed significant similarity (>70% sequence identity) with each other, but considerable dissimilarity (<60% sequence identity) with rhinoviruses in group A [53]. Sequences for all the structural proteins of ten rhinoviruses support the observation derived from the VP2 sequence alone [20,52]. Polioviruses are also associated with antiviral group A, based on their antiviral compound sensitivities, but their amino-acid sequences not only differ from group B rhinoviruses, but also differ considerably from group A rhinoviruses (Table 4).

Various phylogenetic trees showing the relationships among rhinoviruses and polioviruses have been computed based on nucleotide or amino-acid sequences for various genes or gene products [52,53]. The phylogenetic tree based on the amino-acid sequence similarity in VP1 (which contains the residues forming the drug-binding pocket; Fig. 8) demonstrates the separate development of antiviral groups A and B in rhinoviruses and polioviruses. However, the analysis of the phylogenetic trees, derived from VP1, VP2 or the whole structural protein region, does not lead to a clear conclusion on the origin of the major- and minor-receptor group rhinoviruses. It appears that the use of specific receptors may have evolved more than once.

Biological implications

The more than 100 serotypes of human rhinovirus (common cold virus; HRV) can be divided into a major and a minor group based on their use of different receptors. HRV14, HRV3 and HRV16 all belong to the major-receptor group, which uses ICAM-1 as a receptor, whereas HRV1A belongs to the minor-receptor group. HRVs can also be divided into two groups (A and B) based on their sensitivity to a series of capsid-binding antiviral compounds. HRV14 and HRV3 belong to group A, whereas HRV16 and HRV1A belong to group B.

Human rhinovirus 3 (HRV3) was chosen for structural investigations because it is one of a subset of serotypes that best represented the drug sensitivity of most rhinoviruses. It was surprising to find that the sequence and structure of HRV3 was very similar to HRV14, as the latter serotype had previously been found to be an outlier among rhinoviruses. Furthermore, HRV3, like HRV14, but in contrast to all other known structures of HRVs, polioviruses, bovine enterovirus and coxsackievirus B3, did not contain a 'pocket factor' bound within the VP1 β barrel. The pocket factor binds into the same pocket used by the capsid-binding antiviral compounds. It has been suggested that the pocket factor, presumably of cellular origin, regulates the viral life cycle, but its absence in HRV3 and HRV14 indicates that the weakly binding pocket factor may have been removed during purification. Antiviral compounds can displace the pocket factor, thereby interfering in cell attachment or uncoating.

The division of HRVs into major- and minor-receptor groups does not correlate well with sequence or structural similarities. For instance, the major-receptor group

rhinovirus HRV16 has more in common with the minor group rhinovirus HRV1A than with the major group rhinoviruses HRV3 and HRV14. On the other hand, grouping of HRVs by their drug sensitivity does correlate with sequence and structural similarities. Both HRV3 and HRV14 belong to antiviral group A, whereas HRV1A and HRV16 belong to group B.

Although all polioviruses belong to antiviral group A, purified and crystallized polioviruses invariably contain well bound pocket factor unlike HRV3 and HRV14. Comparison of the binding mode of antiviral compounds to these viruses shows considerable similarity in the conformation and position of the compounds. Thus, it is reasonable to assume that a putative pocket factor would bind in HRV3 and HRV14 as it would in polioviruses. However, the environment of the pocket factor in group A rhinoviruses provides poorer hydrophobic interactions compared with polioviruses, explaining the absence of pocket factor in the available structures of group A rhinoviruses.

HRV3, like HRV14, has the first 12 amino acids of VP1 disordered, whereas in the group B rhinoviruses this polyprotein forms an amphipathic helix which interacts with VP4. The greater stability of the group B rhinoviruses in the presence of soluble ICAM-1 or at low pH may result from the stabilizing effects of the amphipathic VP1 helix and the presence of a better bound pocket factor. This higher stability of group B rhinoviruses also correlates with their higher pathogenicity, permitting greater success in transmission from host to host.

Materials and methods

Virus growth, purification and crystallization

HeLa cells were grown in a suspension culture to a concentration of $6\text{--}8 \times 10^5$ cells ml^{-1} . Ten to twelve liters of HeLa cells were harvested by centrifugation at 1600 rpm for 10 min. The pellet was suspended in 3150 ml of medium A (see [54]) plus 350 ml of 10% calf serum. The cells were then distributed evenly among 20 sterilized roller bottles and monolayers formed in 3–5 h. Each bottle was washed with 10–20 ml of PBS buffer and was infected with approximately 9×10^8 PFU of HRV3. 10 ml of AH medium (5.94 g Hepes dissolved in medium A) was then added to each bottle. After 1–2 h of viral attachment, 2.5 ml of both calf serum and AH medium were added to bring the final volume to 50 ml. Bottles were then rolled slowly at 35°C until complete cytopathic effects were observed (≈ 24 h).

The infected cells were frozen and thawed three times and homogenized twice. The suspension was spun at 10K rpm at 5°C for 10 min. PEG 8000 and NaCl were added to the supernatant to achieve a final concentration of 8% (w/v) and 0.5M, respectively. The solution was incubated overnight at 4°C to precipitate the virus. The virus was harvested by spinning at 10K rpm at 5°C for 15 min. The pellet was re-suspended in 30–45 ml of cold 0.25M Hepes/0.75M NaCl/pH 7.2 buffer, and was treated with MgCl_2 (0.005M) and DNase (0.01 mg ml^{-1}) for 30 min at room temperature, followed by 1 mg ml^{-1} trypsin treatment at 35°C for 10 min to inactivate the DNase. After 0.01M NaEDTA (pH 9.5) and 1% sarcosine were added, supernatants were collected following centrifugation at 12K rpm for 10 min at 5°C and then centrifuged through a

30% sucrose cushion at 48K rpm at 5°C for 2 h. The pellet was resuspended and spun through a 10–40% potassium tartrate gradient at 36K rpm at 5°C for 90 min. The resulting virus band was collected and the concentration of the virus was measured by a spectrophotometer using an absorption coefficient of $7.7 \text{ ml}(\text{mg} \times \text{cm})^{-1}$ at 260 nm wavelength. The virus was brought to a final concentration of 10 mg ml^{-1} in preparation for crystallization.

The hanging drop vapor diffusion method was used to crystallize HRV3. The reservoir solution contained 10 mM CaCl_2 and 0.75% PEG 8000 in a 0.25M Hepes/0.75M NaCl/pH 7.2 buffer. The hanging drop contained 5 μl of 10 mg ml^{-1} virus mixed with 5 μl of reservoir solution.

The WIN56291 compound was diffused into HRV3 crystals that had been transferred to 500 μl of stabilization buffer, which was the same as the reservoir solution used in crystallization, except that the PEG 8000 concentration had been increased to 4%. The WIN56291 compound was then dissolved in DMSO to a concentration of 10 mg ml^{-1} . 40 μl of this solution was added to the stabilization buffer that contained the crystals. The crystals were allowed to equilibrate with the WIN compound for at least 24 h before data collection.

Determination of amino-acid sequence of capsid proteins for HRV3

The HRV3 genomic RNA was isolated from purified virions using Proteinase K digestion and phenol:chloroform extraction. The 5' portion of the genomic RNA, covering the viral capsid region, was reverse transcribed to cDNA using Moloney murine leukemia virus (M-MuLV) reverse transcriptase and the primer 5'-GAAATCTTATTAGCAATC-CATTC-3'. The resultant cDNA was amplified using the polymerase chain reaction (PCR) and was cloned into the plasmid vector pCRII using the 'TA' cloning kit (Invitrogen). The two primers used in DNA amplification were 5'-TAGTTTGGTTCGATGAGGCTAGGAATCCCC-3' and 5'-ATCCCACCACAGTCTCCTGGTTCTGCTGGT-3'. A clone that contained the entire capsid coding region was selected by checking the size of the insert and sequencing both ends. Subclones carrying various lengths of the insert were generated from this clone using the 'Erase-a-Base' system (Promega). The two restriction enzymes used to generate the 'substrate' and 'protection' sites in the 'Erase-a-Base' system were NdeI and KpnI, respectively. These subclones were sequenced using the dideoxynucleotide sequencing method [55], and the sequence information was assembled based on the alignment with HRV14 cDNA sequence using the program library of the University of Wisconsin Genetics Computer Group (UWGCG). The remaining gaps between subclones were filled in using primers designed from known sequences. The nucleotide sequence was then translated into the equivalent amino-acid sequence. The nucleotide and amino-acid sequences for the capsid region of HRV3 were found to be 77% and 88% identical, respectively, to HRV14.

Diffraction data collection and processing

The complete HRV3 data set was collected on imaging plates at the F1 station of the Cornell High Energy Synchrotron Source (CHESS) in a single data trip. The wavelength of the F1 station was approximately 0.91 Å. Oscillation angles were chosen to be 0.35° or 0.40° to avoid overlap of reflections at high resolution. The crystal-to-imaging plate distance was 300 mm and the exposure time was about 60 sec. The HRV3 crystals diffracted to 2.8 Å resolution, although the diffraction data were used only to 3.0 Å resolution for the structure solution due to the poor quality of the data at higher resolution. Six to twelve useful exposures could be taken from each crystal before the diffraction showed signs of deterioration.

The imaging plates were indexed using S Kim's auto-indexing program [56]. The cell parameters from different crystals were averaged and used to obtain integrated intensities [57]. Post-refinement [58] was used to refine crystal orientations, cell dimensions and crystal mosaicity. The statistics of the refined data set are given in

Table 5. The cell dimensions after post-refinement were $a = 400.8$, $b = 344.2$, $c = 303.9 \text{ \AA}$, $\alpha = \beta = \gamma = 90^\circ$, assuming a wavelength of 0.9100 \AA .

Space group and structure determination

The indexing program [56] showed HRV3 had a primitive cell with angles close to 90° . The HRV3 crystals were also shown to have mmm symmetry in reciprocal space. Hence, the only possible orthorhombic space groups were $P222$, $P222_1$ (or $P2_122$ or $P22_12$), $P2_12_12$ (or $P22_12_1$ or $P2_122_1$) and $P2_12_12_1$. Two particles per unit cell gave a reasonable V_M value of $2.5 \text{ \AA}^3 \text{ Da}^{-1}$ [59]. Thus, space group $P2_12_12_1$ could be ruled out. Furthermore, only space group $P2_12_12$ (or $P22_12_1$ or $P2_122_1$) could accommodate two viral particle with diameters around 300 \AA in one unit cell. For example, in space group $P2_12_12$ the particles would be placed on twofold axes close to $(0, 0, \frac{1}{4})$ and $(\frac{1}{2}, \frac{1}{2}, \frac{3}{4})$ to reach a maximum separation of 304 \AA .

As there were only two particles in the unit cell, the rotation and translation problem was simplified into a search for the rotation about the crystallographic twofold axis and translation along this axis. A self-rotation function [60] for $\kappa = 72^\circ$, 120° and 180° was calculated with $8\text{--}10 \text{ \AA}$ resolution data and a 150 \AA radius of integration. This showed peaks corresponding to only one icosahedral particle, suggesting that the two particles in the unit cell had a very similar, if not exactly the same, orientation. However, when $3.0\text{--}3.2 \text{ \AA}$ resolution data were used for the rotation function, one threefold peak showed an approximate 1° split representing a rotation about the b axis. Thus, the two particles in the unit cell were related to a particle in the standard orientation by a rotation of 89.5° and 90.5° about a direction parallel to b . As the splitting was about the b axis, the twofold axis must be along b and the correct space group was, therefore, identified as $P2_122_1$.

A stepwise R factor search using $10\text{--}8.5 \text{ \AA}$ resolution data, the previously determined particle orientations and HRV14 as a search model, showed that the two particles were situated at the $(0, 0.2510, 0)$ and $(0.5000, 0.7490, 0.5000)$ positions. This arrangement would lead to a pseudo $I222$ symmetry, which was confirmed by the systematic weakness of the $h + k + l = \text{odd}$ reflections.

The orientation and position of one independent HRV3 particle were refined with the program CLIMB (MGR, unpublished data) using a 4.0 \AA HRV14 map. CLIMB minimizes the density differences between icosahedral symmetry-related points by systematically altering the positional and orientational parameters to optimize the particle orientation and position. Only the rotation angle κ about the b axis and the translation along the b axis were refined. After four cycles of refinement, the orientation and position converged to $(\phi = 0^\circ, \psi = 0^\circ, \kappa = 89.34^\circ)$ and $(0, 0.2504, 0)$, respectively.

A 30 \AA to 4.0 \AA resolution map was calculated using the program ENVELOPE with HRV14 as a phasing model [61]. The map was averaged within a spherical mask that had outer and inner radii of 165 \AA and 70 \AA , respectively. The outside and inside of this mask were considered as solvent and nucleic acid, respectively, and were set to their mean values. Overlapping particles were separated by tangential planes. The

overall correlation coefficient improved from 0.605 to 0.858 after five cycles of averaging.

Resolution of the electron-density map was extended to 3.5 \AA using phases from 30 \AA to 4.2 \AA obtained from the back-transformed averaged map and phases from 4.2 \AA to 3.5 \AA obtained from the known HRV14 model. The resultant map was averaged and solvent flattened using the same spherical mask as had been used for the 30 \AA to 4.0 \AA map. The overall correlation coefficient improved from 0.8561 to 0.9100 after six cycles of averaging.

The 30 \AA to 3.5 \AA map was further extended to 3.0 \AA using the same strategy. Phases for 30 to 3.6 \AA data were obtained from averaging, and phases from 3.6 to 3.0 \AA were obtained from the HRV14 model. After eight cycles of averaging and solvent flattening, the overall correlation coefficient improved from 0.846 to 0.880.

Pseudo higher order space groups are not uncommon for icosahedral virus crystals [62–64]. In these circumstances, the quality of phasing of the 'odd' (weak) reflections is very sensitive to correct determination of the orientational and positional parameters. Indeed, a wrong determination of space group or inaccurate parameter determination results in very poor correlation coefficients for 'odd' reflections without affecting significantly the 'even' reflections. The correctness of the current structure determination is, therefore, indicated by the 0.93 and 0.84 correlation coefficients for the $h + k + l = 2n$ and $2n + 1$ reflections, respectively, between 30 \AA and 8 \AA resolution [49].

Wavelength adjustment and preliminary refinement

The amino acids of HRV3 capsid proteins were built into the map using the graphics program O [65]. The model of the HRV3 structure was found to be systematically expanded with respect to the corresponding 2.4 \AA resolution refined HRV14 structure (B Berger and MGR, unpublished results) as shown by plots of differences in the x, y, z coordinates as a function of the mean value of x, y or z , respectively (Fig. 9). Similar plots comparing HRV1A and HRV14 gave no significant differences. The correct cell dimensions of cubic HRV14 had been established using $\text{CuK}\alpha$ radiation [49]. Apparently, the bond lengths of HRV3 were systematically larger than those of HRV14. A possible explanation for this phenomenon was that the wavelength used for processing the HRV3 data was bigger than it should have been due to the inaccuracy of the synchrotron X-ray wavelength determination. This would imply that the cell dimensions determined by post-refinement, assuming a wavelength of 0.9100 \AA , were 1.007 times too big, as suggested by the slope of the curve in Figure 9. Hence, the cell dimensions were corrected to $a = 397.9$, $b = 341.8$, $c = 301.7 \text{ \AA}$ and these were used for further refinement. Lea *et al.* [66] and Curry *et al.* [67] have used similar procedures to calibrate the wavelength of the synchrotron radiation.

A preliminary refinement of HRV3 coordinates was performed using the energy minimization routine of the program X-PLOR [68]. For $5.0\text{--}3.0 \text{ \AA}$ resolution data, the final R factor calculated using the refined coordinates with an overall B factor of 15 \AA^2 was 28.1%. The rms deviations from the ideal bond lengths and bond angles were 0.009 \AA and 1.8° , respectively. R_{free} is not a useful indicator in the presence of high

Table 5

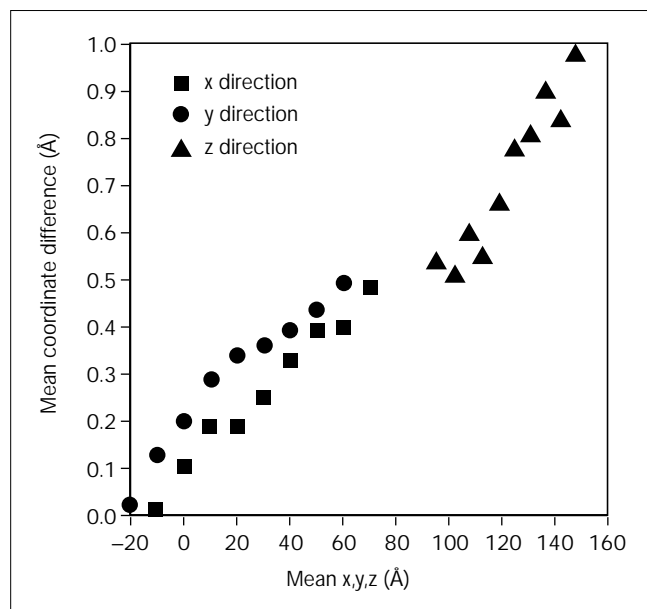
Statistics on the diffraction data of native HRV3.*

Resolution (\AA)	30–25	25–12.5	12.5–8.33	8.33–6.25	6.25–5.00	5.00–4.17	4.17–3.57	3.57–3.12	3.12–2.80
No. of reflections	430	8074	24 206	45 589	75 728	112 936	147 856	176 196	139 901
Data (%)	73	82	91	88	88	89	82	73	47
R_{merge}	7.42	9.75	9.31	11.81	11.37	10.11	11.96	14.89	18.90

*Number of imaging plates, 331; number of crystals, 45; cutoff criteria = $F_h^2 > 3\sigma(F_h^2)$; number of measurements, 1 917 753; number

of unique reflections, 730 925; overall completeness, 73.1%; overall R_{merge} , 12.0%.

Figure 9



Relationship between the $C\alpha$ -coordinate differences (HRV3–HRV14) and the coordinates of these atoms, prior to wavelength adjustment.

non-crystallographic symmetry, because of the interdependence of structure factors [69].

Structure determination of HRV3 complexed with WIN56291

An electron-density map was calculated with Fourier coefficient $(F_D - kF_N) \omega_N \exp(i\alpha_N)$ [16]. F_D and F_N are the structure factor amplitudes of the drug–virus complex and of the native virus placed onto the same relative scale, respectively; α_N is the phase for the native structure obtained from the molecular replacement and real-space averaging procedure; ω_N is the weighting factor dependent on the consistency between the $F_N(\text{obs})$ and $F_N(\text{calc})$ obtained in the averaging procedure used to determine phases of the native structure; and k is a suitably chosen scale factor. A simple difference map with $k = 1$ was calculated to locate conformational changes due to the drug binding to HRV3. A map with $k = 0.7$ was calculated to interpret the actual drug and protein conformations in the virus–drug complex. In this map, the density level of the drug was similar to the density level of the surrounding protein and the effects of the incomplete substitution and phase bias toward native structure were minimized. The difference map was averaged using the 30-fold noncrystallographic redundancy in HRV3 crystals [61]. An atomic model was built into the averaged map using the graphics program O [65]. The coordinates of this model were also shrunk as discussed in the section on ‘Wavelength adjustment and preliminary refinement’.

Accession numbers

The coordinates have been deposited with the Brookhaven Protein Data Bank (code 1RHI). The cDNA sequence has been deposited with the Gene Bank (accession number U60874).

Acknowledgements

We are grateful to many members of our laboratory and to the CHES staff in helping with the data collection and to Cheryl Towell and Sharon Wilder for help in preparation of this paper. We thank Roland Rueckert and Wai-Ming Lee for useful discussions. The work was funded by grants to MGR from the National Institute of Health and the former Sterling–Winthrop Pharmaceutical Research Division. A Lucille P Markey Foundation Award to MGR provided additional facilities for the structural biology faculty at Purdue University.

References

- Abraham, G. & Colonno, R.J. (1984). Many rhinovirus serotypes share the same cellular receptor. *J. Virol.* **51**, 340–345.
- Greve, J.M., *et al.*, & McClelland, A. (1989). The major human rhinovirus receptor is ICAM-1. *Cell* **56**, 839–847.
- Staunton, D.E., Merluzzi, V.J., Rothlein, R., Barton, R., Marling, S.D. & Springer, T.A. (1989). A cell adhesion molecule, ICAM-1, is the major surface receptor for rhinoviruses. *Cell* **56**, 849–853.
- Uncapher, C.R., DeWitt, C.M. & Colonno, R.J. (1991). The major and minor group receptor families contain all but one human rhinovirus serotype. *Virology* **180**, 814–817.
- Hofer, F., *et al.*, & Blaas, D. (1994). Members of the low density lipoprotein receptor family mediate cell entry of a minor-group common cold virus. *Proc. Natl. Acad. Sci. USA* **91**, 1839–1842.
- Rossmann, M.G., *et al.*, & Vriend, G. (1985). Structure of a human common cold virus and functional relationship to other picornaviruses. *Nature* **317**, 145–153.
- Oliveira, M.A., *et al.*, & Rossmann, M.G. (1993). The structure of human rhinovirus 16. *Structure* **1**, 51–68.
- Kim, S., *et al.*, & McKinlay, M.A. (1989). The crystal structure of human rhinovirus serotype 1A (HRV1A). *J. Mol. Biol.* **210**, 91–111.
- Rossmann, M.G. & Palmenberg, A.C. (1988). Conservation of the putative receptor attachment site in picornaviruses. *Virology* **164**, 373–382.
- Chapman, M.S. & Rossmann, M.G. (1993). Comparison of surface properties of picornaviruses: strategies for hiding the receptor site from immune surveillance. *Virology* **195**, 745–756.
- Rossmann, M.G. (1994). Viral cell recognition and entry. *Protein. Sci.* **3**, 1712–1725.
- Colonno, R.J., Condra, J.H., Mizutani, S., Callahan, P.L., Davies, M.E. & Murcko, M.A. (1988). Evidence for the direct involvement of the rhinovirus canyon in receptor binding. *Proc. Natl. Acad. Sci. USA* **85**, 5449–5453.
- Olson, N.H., *et al.*, & Rossmann, M.G. (1993). Structure of a human rhinovirus complexed with its receptor molecule. *Proc. Natl. Acad. Sci. USA* **90**, 507–511.
- Sherry, B., Mosser, A.G., Colonno, R.J. & Rueckert, R.R. (1986). Use of monoclonal antibodies to identify four neutralization immunogens on a common cold picornavirus, human rhinovirus 14. *J. Virol.* **57**, 246–257.
- Smith, T.J., *et al.*, & Baker, T.S. (1993). Structure of human rhinovirus complexed with Fab fragments from a neutralizing antibody. *J. Virol.* **67**, 1148–1158.
- Smith, T.J., *et al.*, & Otto, M.J. (1986). The site of attachment in human rhinovirus 14 for antiviral agents that inhibit uncoating. *Science* **233**, 1286–1293.
- Badger, J., *et al.*, & Heinz, B.A. (1988). Structural analysis of a series of antiviral agents complexed with human rhinovirus 14. *Proc. Natl. Acad. Sci. USA* **85**, 3304–3308.
- Kim, K.H., *et al.*, & Pevear, D.C. (1993). A comparison of the anti-rhinoviral drug binding pocket in HRV14 and HRV1A. *J. Mol. Biol.* **230**, 206–225.
- Pevear, D.C., *et al.*, & Dutko, F.J. (1989). Conformational change in the floor of the human rhinovirus canyon blocks adsorption to HeLa cell receptors. *J. Virol.* **63**, 2002–2007.
- Andries, K., *et al.*, & Janssen, P.A.J. (1990). Two groups of rhinoviruses revealed by a panel of antiviral compounds present sequence divergence and differential pathogenicity. *J. Virol.* **64**, 1117–1123.
- Hogle, J.M., Chow, M. & Filman, D.J. (1985). Three-dimensional structure of poliovirus at 2.9 Å resolution. *Science* **229**, 1358–1365.
- Filman, D.J., Syed, R., Chow, M., Macadam, A.J., Minor, P.D. & Hogle, J.M. (1989). Structural factors that control conformational transitions and serotype specificity in type 3 poliovirus. *EMBO J.* **8**, 1567–1579.
- Yeates, T.O., *et al.*, & Hogle, J.M. (1991). Three-dimensional structure of a mouse-adapted type 2/type 1 poliovirus chimera. *EMBO J.* **10**, 2331–2341.
- Smyth, M., Tate, J., Hoey, E., Lyons, C., Martin, S. & Stuart, D. (1995). Implications for viral uncoating from the structure of bovine enterovirus. *Nat. Struct. Biol.* **2**, 224–231.
- Muckelbauer, J.K., *et al.*, & Rossmann, M.G. (1995). The structure of coxsackievirus B3 at 3.5 Å resolution. *Structure* **3**, 653–667.
- Gruenberger, M., Pevear, D., Diana, G.D., Kuechler, E. & Blaas, D. (1991). Stabilization of human rhinovirus serotype 2 against pH-induced conformational change by antiviral compounds. *J. Gen. Virol.* **72**, 431–433.
- Fox, M.P., Otto, M.J. & McKinlay, M.A. (1986). The prevention of rhinovirus and poliovirus uncoating by WIN 51711: a new antiviral drug. *Antimicrob. Agents Chemother.* **30**, 110–116.

28. Heinz, B.A., *et al.*, & Smith, T.J. (1989). Genetic and molecular analyses of spontaneous mutants of human rhinovirus 14 that are resistant to an antiviral compound. *J. Virol.* **63**, 2476–2485.
29. Bibler-Muckelbauer, J.K., *et al.*, & McKinlay, M.A. (1994). Human rhinovirus 14 complexed with fragments of active antiviral compounds. *Virology* **202**, 360–369.
30. Morton, A., Baase, W.A. & Matthews, B.W. (1995). Energetic origins of specificity of ligand binding in an interior nonpolar cavity of T4 lysozyme. *Biochemistry* **34**, 8564–8575.
31. Eriksson, A.E., Baase, W.A., Wozniak, J.A. & Matthews, B.A. (1992). A cavity-containing mutant of T4 lysozyme is stabilized by buried benzene. *Nature* **355**, 371–373.
32. Eriksson, A.E., *et al.*, & Matthews, B.W. (1992). Response of a protein structure to cavity-creating mutations and its relation to the hydrophobic effect. *Science* **255**, 178–183.
33. DeSana, J. & Mandell, B. (1977). Studies on the *in vitro* uncoating of poliovirus. II. Characterization of the membrane-modified particle. *Virology* **78**, 554–566.
34. Lonberg-Holm, K. & Korant, B.D. (1972). Early interaction of rhinoviruses with host cells. *J. Virol.* **9**, 29–40.
35. Hoover-Litty, H. & Greve, J.M. (1993). Formation of rhinovirus-soluble ICAM-1 complexes and conformational changes in the virion. *J. Virol.* **67**, 390–397.
36. Korant, B.D., Lonberg-Holm, K., Yin, F.H. & Noble-Harvey, J. (1975). Fractionation of biologically active and inactive populations of human rhinovirus type 2. *Virology* **63**, 384–394.
37. Fricks, C.E. & Hogle, J.M. (1990). Cell-induced conformational change in poliovirus: externalization of the amino terminus of VP1 is responsible for liposome binding. *J. Virol.* **64**, 1934–1945.
38. Jaeger, E.P., Pevear, D.C., Felock, P.J., Russo, G.R. & Treasurywala, A.M. (1995). Genetic algorithm based method to design a primary screen for antirhinovirus agents. In *Computer-Aided Molecular Design: Applications in Agrochemicals, Materials, and Pharmaceuticals*. (Reynolds, C.H., Holloway, M.K. & Cox, H.K., eds), pp. 139–155, American Chemical Society, Washington D.C., USA.
39. Murray, M.G., Bradley, J., Yang, X.-F., Wimmer, E., Moss, E.G. & Racaniello, V.R. (1988). Poliovirus host range is determined by a short amino acid sequence in neutralization antigenic site I. *Science* **241**, 213–215.
40. Murray, M.G., Kuhn, R.J., Arita, M., Kawamura, N., Nomoto, A. & Wimmer, E. (1988). Poliovirus type 1/type 3 antigenic hybrid virus constructed *in vitro* elicits type 1 and type 3 neutralizing antibodies in rabbits and monkeys. *Proc. Natl. Acad. Sci. USA* **85**, 3203–3207.
41. Burke, K.L., Dunn, G., Ferguson, M., Minor, P.D. & Almond, J.W. (1988). Antigen chimeras of poliovirus as potential new vaccines. *Nature* **332**, 81–82.
42. Murrin, A.D. & Wimmer, E. (1989). Construction of a poliovirus type 1/type 2 antigenic hybrid by manipulation of neutralizing antigenic site II. *J. Virol.* **63**, 5251–5257.
43. Evans, D.J., *et al.*, & Almond, J.W. (1989). An engineered poliovirus chimaera elicits broadly reactive HIV-1 neutralizing antibodies. *Nature* **339**, 385–388.
44. Jenkins, O., *et al.*, & Almond, J.W. (1990). An antigen chimera of poliovirus induces antibodies against human papillomavirus type 16. *J. Virol.* **64**, 1201–1206.
45. Ansardi, D.C., Porter, D.C. & Morrow, C.D. (1992). Myristylation of poliovirus capsid precursor P1 is required for assembly of subviral particles. *J. Virol.* **66**, 4556–4563.
46. Chow, M., Newman, J.F.E., Filman, D., Hogle, J.M., Rowlands, D.J. & Brown, F. (1987). Myristylation of picornavirus capsid protein VP4 and its structural significance. *Nature* **327**, 482–486.
47. Lee, W.M., Monroe, S.S. & Rueckert, R.R. (1993). Role of maturation cleavage in infectivity of picornaviruses: activation of an infectious. *J. Virol.* **67**, 2110–2122.
48. Zhao, R., Hadfield, A.T., Kremer, M.J. & Rossmann, M.G. (1996). Cations in human rhinoviruses. *Virology*, in press.
49. Arnold, E. & Rossmann, M.G. (1990). Analysis of the structure of a common cold virus, human rhinovirus 14, refined at a resolution of 3.0 Å. *J. Mol. Biol.* **211**, 763–801.
50. Ohlin, A., *et al.*, & Greve, J.M. (1994). Spectrum of activity of soluble intercellular adhesion molecule-1 against rhinovirus reference strains and field isolates. *Antimicrob. Agents Chemother.* **38**, 1413–1415.
51. Hiremath, C.N., Grant, R.A., Filman, D.J. & Hogle, J.M. (1995). Binding of the antiviral drug WIN51711 to the Sabin strain of type 3 poliovirus: structural comparison with drug binding in rhinovirus 14. *Acta Crystallogr. D* **51**, 473–489.
52. Palmenberg, A.C. (1989). Sequence alignments of picornaviral capsid proteins. In *Molecular Aspects of Picornavirus Infection and Detection*. (Semler, B.L. & Ehrenfeld, E., eds), pp. 211–241, American Society for Microbiology, Washington D.C., USA.
53. Horsnell, C., Gama, R.E., Hughes, P.J. & Stanway, G. (1995). Molecular relationships between 21 human rhinovirus serotypes. *J. Gen. Virol.* **76**, 2549–2555.
54. Medappa, K.C., McLean, C. & Rueckert, R.R. (1971). On the structure of rhinovirus 1A. *Virology* **44**, 259–270.
55. Sanger, F., Nicklin, S. & Coulson, A.R. (1977). DNA sequencing with chain-termination inhibitors. *Proc. Natl. Acad. Sci. USA* **74**, 5463–5467.
56. Kim, S. (1989). Auto-indexing oscillation photographs. *J. Appl. Crystallogr.* **22**, 53–60.
57. Rossmann, M.G. (1979). Processing oscillation diffraction data for very large unit cells with an automatic convolution technique and profile fitting. *J. Appl. Crystallogr.* **12**, 225–238.
58. Rossmann, M.G., Leslie, A.G.W., Abdel-Meguid, S.S. & Tsukihara, T. (1979). Processing and post-refinement of oscillation camera data. *J. Appl. Crystallogr.* **12**, 570–581.
59. Matthews, B.W. (1968). Solvent content of protein crystals. *J. Mol. Biol.* **33**, 491–497.
60. Rossmann, M.G. & Blow, D.M. (1962). The detection of sub-units within the crystallographic asymmetric unit. *Acta Crystallogr.* **15**, 24–31.
61. Rossmann, M.G., *et al.*, & Choi, H.-K. (1992). Molecular replacement real-space averaging. *J. Appl. Crystallogr.* **25**, 166–180.
62. Muckelbauer, J.K., *et al.*, & Rossmann, M.G. (1995). Structure determination of coxsackievirus B3 to 3.5 Å resolution. *Acta Crystallogr. D* **51**, 871–887.
63. Zlotnick, A., McKinney, B.R., Munshi, S., Bibler, J., Rossmann, M.G. & Johnson, J.E. (1993). A monoclinic crystal with R32 pseudo-symmetry: a preliminary report of nodamura virus structure determination. *Acta Crystallogr. D* **49**, 580–587.
64. Llamas-Saiz, A.L., Agbandje-McKenna, M., Wikoff, W.R., Tattersall, P., Bratton, J. & Rossmann, M.G. (1996). Structure determination of minute virus of mice. *Acta Crystallogr.*, in press.
65. Jones, T.A., Zou, J.-Y., Cowan, S.W. & Kjeldgaard, M. (1991). Improved methods for building protein models in electron density maps and the location of errors in these models. *Acta Crystallogr. A* **47**, 110–119.
66. Lea, S., *et al.*, & Mateu, M.G. (1994). The structure and antigenicity of a type C foot-and-mouth disease virus. *Structure* **2**, 123–139.
67. Curry, S., *et al.*, & Stuart, D. (1996). Perturbations in the surface structure of A22 Iraq foot-and-mouth disease virus accompanying coupled changes in host cell specificity and antigenicity. *Structure* **4**, 135–145.
68. Brünger, A.T. (1993). *X-PLOR, Version 3.1 Manual: A System for X-Ray Crystallography and NMR*. Yale University Press, New Haven, USA.
69. Chapman, M.S. & Rossmann, M.G. (1996). Structural refinement of the DNA-containing capsid of canine parvovirus using RSRef, a resolution-dependent stereochemically restrained real-space refinement method. *Acta Crystallogr. D* **52**, 129–140.